Scanning Microscopy

Volume 6 | Number 4 Article 8

10-5-1992

Modelling Techniques for the Quantification of Some Electron Beam Induced Phenomena

WK Chim
National University of Singapore

DSH Chan
National University of Singapore

TS Low
National University of Singapore

JCH Phang
National University of Singapore

KS Sim
National University of Singapore

See next page for additional authors

Modelling Techniques for the Quantification of Some Electron Beam Induced Phenomena

Authors
WK Chim, DSH Chan, TS Low, JCH Phang, KS Sim, and KL Pey

Scanning Microscopy, Vol. 6, No. 4, 1992 (Pages 961-978) 0891-7035/92$5.00+.00
Scanning Microscopy International, Chicago (AMF O'Hare), IL 60666 USA

MODELLING TECHNIQUES FOR THE QUANTIFICATION OF SOME ELECTRON BEAM INDUCED PHENOMENA

WK Chim, DSH Chan*, TS Low, JCH Phang, KS Sim and KL Pey
Centre for Integrated Circuit Failure Analysis and Reliability
Faculty of Engineering, National University of Singapore
10 Kent Ridge Crescent, Singapore 0511
Republic of Singapore

(Received for publication April 18, 1992, and in revised form October 5, 1992)

Abstract

This paper presents simulation models for quantifying the voltage contrast, cathodoluminescence and indirect specimen charging phenomena in the scanning electron microscope (SEM). The voltage contrast model comprises an electric field computation program using the finite-element approach, and a secondary electron trajectory tracking algorithm employing a linear electric field assumption. This trajectory tracking algorithm is more accurate than the conventional electron trajectory tracking algorithms which make use of a constant electric field assumption within each computation step. Using this model, results of qualitative voltage contrast effects on secondary electron trajectories in the specimen chamber of the SEM are shown. This model can also be used for quantitative voltage studies for designing low error voltage energy analysers. The cathodoluminescence (CL) model consists of programs for simulating the electron beam-specimen interaction via Monte Carlo analysis, excess carrier generation and distribution, and optical losses of the CL emission. This model has been used to simulate the CL intensity as a function of surface recombination velocity, diffusion length, and absorption coefficient. A model has also been developed to simulate indirect charging of specimens in the SEM. This model uses the finite-element method to solve for the self-consistent electric field due to the imposed boundary conditions, trapped and moving charges. Secondary electrons are tracked using the trajectory tracking scheme developed.

Key Words: Simulation models, electron beam induced phenomena, voltage contrast, cathodoluminescence, specimen charging, scanning electron microscope, trajectory tracking algorithms, finite-element method, Monte Carlo analysis, low error voltage energy analysers.

* Address for correspondence:
DSH Chan, Department of Electrical Engineering
National University of Singapore
10 Kent Ridge Crescent
Singapore 0511

Phone No.: (65)772-2117
Fax No. : (65)779-1103

Introduction

The scanning electron microscope (SEM) is an important and indispensable tool for the microelectronics industry, especially in the area of integrated circuit failure analysis and material characterization. Besides the advantages of higher resolution and greater depth of field compared to the conventional optical microscope, it also provides a vast spectrum of functional as well as physical information simultaneously using different imaging modes or techniques. These imaging modes include voltage contrast, cathodoluminescence, magnetic contrast and electron beam induced current.

Voltage contrast (VC) imaging, through the use of secondary electron (SE) emission, allows the determination of voltages on a device biased up in the SEM. This technique holds a great deal of promise for quantitative voltage measurements on submicron devices provided the inherent errors in the measurements can be minimised or corrected for. The common modes of operation of voltage contrast are qualitative VC [12,47], quantitative VC [10,18,41,42,43,44,59], dynamic or stroboscopic VC [1,17,40,50] and capacitive coupling VC [19].

Cathodoluminescence (CL) is the emission of light as a result of electron beam bombardment. The emitted light provides information on the luminescent properties of the material or device under test. This technique has been applied extensively for the failure analysis of optoelectronic devices [48], characterization of luminescent centres, defects, radiative and non-radiative recombination processes [26,27].

The magnetic microstructure of materials can be observed in the SEM using the magnetic contrast (MC) imaging mode [63,65,69]. Magnetic contrast is very similar to the voltage contrast phenomenon, except that trajectories of the low energy secondary electrons are influenced by the resultant magnetic fields above the specimen surface for the former rather than electric fields as in voltage contrast.

Electron beam induced current (EBIC) imaging is useful for the detection of junction defects and dopant inhomogeneities [39,53,54] and the measurement of depletion layer widths [53], minority carrier lifetime [3,64] and diffusion length [29,30]. The EBIC current is a charge

multiplication current and is many times that of the absorbed sample current. This is because a single high energy primary electron usually gives rise to thousands of electron-hole pairs in the sample. The recombination of the electron-hole pairs across a junction gives rise to the EBIC current.

To apply the various SEM techniques effectively, one requires a thorough understanding of the fundamental mechanisms of signal generation, detection and the resultant errors limiting the measurement accuracy of each technique. Modelling and computer simulation of the electron beam induced phenomenon are important as they provide physical insights to the fundamental mechanisms behind each technique leading to the theoretical quantification of the detected signal and its inherent errors. This paper reports on the modelling techniques which have been applied for simulating three electron beam induced phenomena, namely voltage contrast, cathodoluminescence and indirect specimen charging. Results of computer simulation showing the applications of these three models are presented.

SEM Voltage Contrast

Background

The optimum conditions for observation of voltage contrast signals in the SEM have to be studied so as to enable the design of efficient voltage contrast detectors. This study will be facilitated with a knowledge of the trajectories of the secondary electrons (SE) emitted by the specimen under test.

The computation of the SE trajectories in the SEM has been addressed by various authors [33,35,43]. Kursheed and Dinnis [35] used the finite difference method to calculate the potential field distribution in the region of interest and then calculated the electron trajectories by a variable step method. They assumed that each trajectory was composed of linear segments. Along each segment, a constant electric field was assumed. The length of each segment was then varied until a specified accuracy was achieved. Nakamae et. al. [43] also made use of the finite difference method to solve the potential field distribution. Although the trajectory tracking algorithm was not discussed, it seemed likely that the method employed assumed a constant electric field between adjacent points of travel of the electron. From our studies, we have found that the computed electron trajectories may be subjected to large errors in some of the common algorithms used, especially in situations of low electron energy and abrupt electric field changes [11].

This section presents a SE trajectory algorithm, coupled to a finite element solver, which overcomes some of the inaccuracies that are associated with the assumption of a constant electric field. In this algorithm, the electric field is assumed to vary linearly with distance within each mesh.

Finite-element calculation of potential field distribution

The potential distribution inside the specimen chamber of the SEM can be modelled by a Poissonian field. This model can be further simplified to that of the Laplacian field distribution since sources of charge generation are essentially negligible in the specimen chamber.

The potential field distribution (ϕ) inside the SEM specimen chamber or that of an energy analyser model is solved for the appropriate boundary conditions using a finite-element program [8,9,11]. The advantages of using the finite-element method over the more commonly used finite difference method have been discussed [11]. In the finite-element solution of a partial differential equation, a geometrically complex domain is represented as a collection of geometrically simpler subdomains called finite elements [52,70]. The differential equation of interest, i.e. Laplace's equation in a two-dimensional space in this case, is put into an equivalent variational form. The solution in each element is assumed to be a combination of interpolation functions, L_i, i.e. $\phi = L_i\phi_i$. The parameters, i.e. ϕ_i, represent the values of the solution at a finite number of preselected nodes on the boundary and in the interior of the element. From interpolation theory, one finds that the order (or degree) of the interpolation function depends on the number of nodes in the element.

A mesh generation programs is used to discretise the region of interest into triangular finite elements. Triangular elements are chosen because they are the simplest polygonal figures into which a two dimensional region can be subdivided and they could also be readily adapted to irregular boundaries. Rectangular elements, on the other hand, are not suited to irregular two-dimensional regions while higher order polygons would lead to additional complexity with only marginal improvements in accuracy.

A secondary electron tracking algorithm

This algorithm (called Algorithm C) is an original model developed to address the inaccuracies and limitations of algorithms which assume a constant electric field between adjacent points of travel of the electron. The algorithm attempts a more realistic representation of the electric field by assuming that it varies linearly with distance within a mesh. The x-component of the electric field is assumed to vary linearly with y while the y-component is assumed to vary linearly with x. The equations of motion then become:

$$(d^2x/dt^2) = K\,(A_x y + B_x) \tag{1}$$

$$(d^2y/dt^2) = K\,(A_y x + B_y) \tag{2}$$

where $K = (q/m)$

Fig. 1 shows the nomenclature for potentials and dimensions in a typical rectangular mesh, made up of two triangular finite elements.

Referring to Fig. 1, the values of A_x, A_y, B_x, and B_y within each mesh are given by:

$$B_x = (V_1 - V_2) / x_m \tag{3}$$

$$A_x = [(V_3 - V_4) / (x_m y_m)] - [B_x/y_m] \tag{4}$$

$$B_y = (V_1 - V_3) / y_m \tag{5}$$

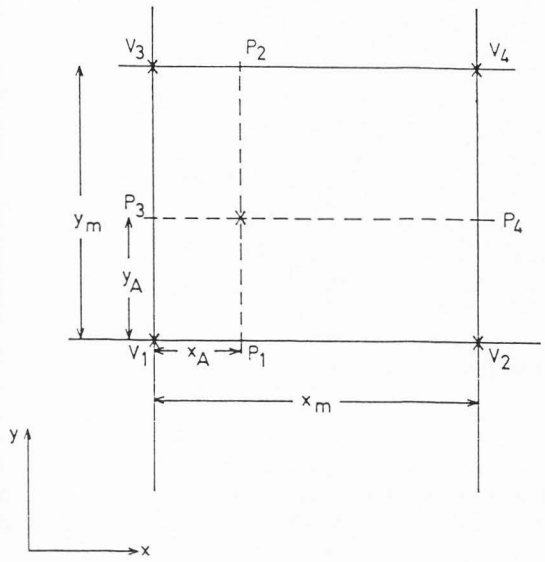

Fig. 1. Potentials and dimensions in a typical mesh.

$$A_y = [(V_2 - V_4) / (x_m y_m)] - [B_y/x_m] \quad (6)$$

From eqn. (2),

$$x = [(1/A_y K)\,(d^2y/dt^2)] - (B_y/A_y) \quad (7)$$

By differentiating eqn. (7) twice and substituting the result into eqn. (1), the following equation, describing the y-motion of the electron, is obtained:

$$(d^4y/dt^4) - (K^2A_xA_y)y = K^2A_yB_x \quad (8)$$

Another equation describing the x-motion of the electron can also be obtained by a similar procedure starting from eqn. (1). The result is:

$$(d^4x/dt^4) - (K^2A_xA_y)x = K^2A_xB_y \quad (9)$$

Both eqns. (8) and (9) can be expressed in the following general form:

$$(d^4y/dt^4) + ay = g_1 \quad (10)$$

$$(d^4x/dt^4) + ax = g_2 \quad (11)$$

where $a = - K^2A_xA_y$

$g_1 = K^2A_yB_x$

$g_2 = K^2A_xB_y$

By using the method of Laplace Transform, both eqns. (10) and (11) can be solved [58]. For example, the solution for eqn. (10) is as follows:

$$y(t) = A(t)y(0) + B(t)y'(0) + C(t)y''(0) + D(t)y'''(0) + F(t) \quad (12)$$

The expressions for A(t), B(t), C(t), D(t) and F(t) depend on whether the value of a in eqn. (10) is positive or negative.

For $a < 0$ and defining p as $\sqrt[4]{|a|}$ gives

$$A(t) = [\cosh(pt) + \cos(pt)] / 2$$

$$B(t) = [\sinh(pt) + \sin(pt)] / (2p)$$

$$C(t) = [\cosh(pt) - \cos(pt)] / (2p^2)$$

$$D(t) = [\sinh(pt) - \sin(pt)] / (2p^3)$$

$$F(t) = (g_1/a)\,[1 - A(t)] \quad (13)$$

For $a > 0$ and defining p as $\sqrt[4]{a/4}$ gives

$$A(t) = \cosh(pt)\cos(pt)$$

$$B(t) = [\sin(pt)\cosh(pt) + \cos(pt)\sinh(pt)] / (2p)$$

$$C(t) = [\sin(pt)\sinh(pt)] / (2p^2)$$

$$D(t) = [\sin(pt)\cosh(pt) - \cos(pt)\sinh(pt)] / (4p^3)$$

$$F(t) = (g_1/a)\,[1 - A(t)] \quad (14)$$

A similar solution also exists for eqn. (11) by replacing all y's by x's in eqn. (12) and g_1 by g_2. The initial conditions for both the x and y motions in each mesh are as follows:

x-motion

$x(0)$ = Initial x-position with respect to the bottom left hand corner of the mesh

$x'(0)$ = Initial velocity in the x-direction

$x''(0) = K[B_x + A_xy(0)]$

$x'''(0) = KA_xy'(0)$ (15)

y-motion

$y(0)$ = Initial y-position with respect to the bottom left hand corner of the mesh

$y'(0)$ = Initial velocity in the y-direction

$y''(0) = K[B_y + A_yx(0)]$

$y'''(0) = KA_yx'(0)$ (16)

The trajectory of the electron is charted within a mesh

by substituting suitable values of t into the equations. The values chosen must always be smaller than the time required for the electron to traverse the mesh since these equations of motion are valid for only one particular mesh and the neighbouring mesh will have a different set of coefficients. The essence of the routine is to determine the point at which the electron leaves the mesh by an analytical solution of the equations of motion which takes into account a linearly varying electric field within the mesh. Since equations (12) to (16) are closed form solutions, the accuracy of the trajectory is independent of the value of the time step chosen provided the electron is confined within the mesh.

Some modifications have been made to the original algorithm reported in [11] to reduce the errors during electron transition between meshes and to make the program more robust. The first is a self-checking function to make sure that the initial value of t chosen is not so large as to cause the electron to cross into an adjacent mesh within this initial time step. If the initial value of t is found to be too large for a particular mesh, it is automatically reduced by the program. The second modification involves fine tuning the value of t until it corresponds to the value which causes the electron to a exit a particular mesh into a neighbouring one. This point of exit of the electron from the present mesh into an adjacent one is found by progressively adjusting the value of t by the half-interval method. This is done until the computed position of the electron from the mesh edge of transition is within the accuracy or tolerance specified. The third modification involves setting a maximum number of iterations for the half-interval loop computation. If the specified accuracy is not met after this maximum number, the last value of computation is taken to be adjusted time t. This is to account for situations where the value of the tolerance set is too small, causing an underflow error during the half-interval loop computation, and also to reduce the computation time.

Qualitative voltage contrast studies in the SEM

Qualitative studies of the voltage contrast effect can be conducted by varying the detector bias, SE energy, specimen tilt and specimen bias one at a time and noting the effect on the SE trajectories and the cone of SE collection. Some results which illustrate the salient features of the trajectory tracking algorithm (i.e. algorithm C) are presented here. As a comparison, results of two constant electric field algorithms (called algorithm A and B) are also shown to highlight the accuracy of algorithm C. Algorithm A makes use of a constant time step and a constant electric field during the step while Algorithm B makes use of a fixed mesh step and a constant electric field within the mesh [11].

In the following simulation plots of SE trajectories in the SEM specimen chamber, the solid lines represent equipotential which are plotted at one volt intervals, while the dotted lines are the SE trajectories for various angles of emission from 0 to 180 degrees at 10 degree intervals.

The sensitivity of algorithm A to the chosen time step is illustrated in Figs. 2 and 3. These plots are obtained for a specimen bias of 3 V, specimen tilt of 0 degrees, detector bias of 10 V and a SE energy of 2 eV. The time steps

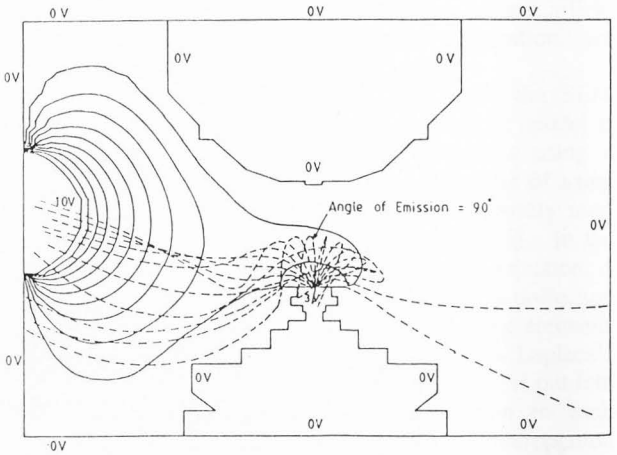

Fig. 2. Application of Algorithm A to electron trajectory tracking in a SEM. (Time step = $1x10^{-8}$ seconds, Specimen Bias = 3.0 V, Detector Bias = 10 V, Secondary Electron Energy = 2 eV).

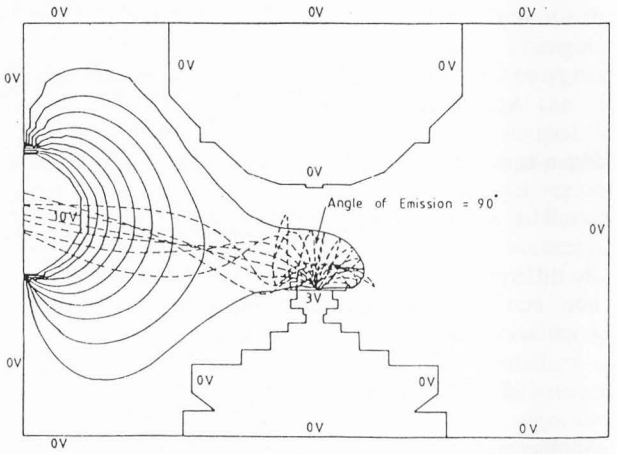

Fig. 3. Application of Algorithm A to electron trajectory tracking in a SEM. (Time step = $5x10^{-10}$ seconds, specimen Bias = 3.0 V, Detector Bias = 10 V, Secondary Electron Energy = 2 eV).

used in obtaining Figs. 2 and 3 are 1 x 10^{-8} seconds and 5 x 10^{-10} seconds respectively, the smaller time step giving a more accurate solution. This can be easily observed by comparing the trajectory of the electron which is emitted at 90 degrees in both figures. In Fig. 2 (the one with the larger time step), the 2 eV electron is turned back towards the specimen before it has overcome a 2 V potential barrier. One would expect an electron of 2 eV energy to have sufficient energy to overcome a 2 V potential barrier before being turned back, and this is what happens in Fig. 3 when a smaller time step is used.

Fig. 4 shows the electron trajectories obtained by algorithm B for the same conditions as in Figs. 2 and 3. It is noted that algorithm B gives a reasonably accurate solution in this case (the 2 eV electron overcoming a potential barrier of 2 V before being turned back towards

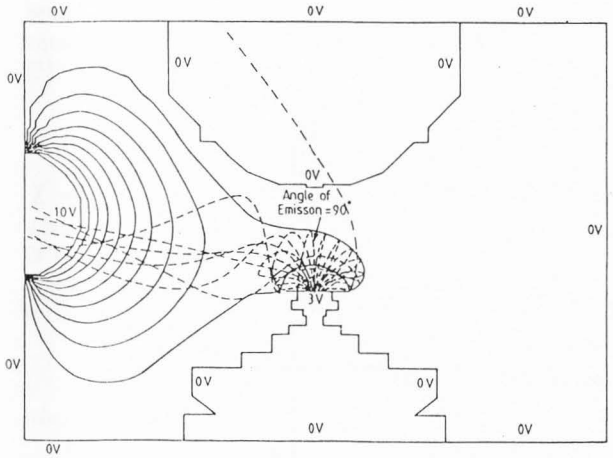

Fig. 4. Application of Algorithm B to electron trajectory tracking in a SEM. (Specimen Bias = 3.0 V, Detector Bias = 10 V, Secondary Electron Energy = 2 eV).

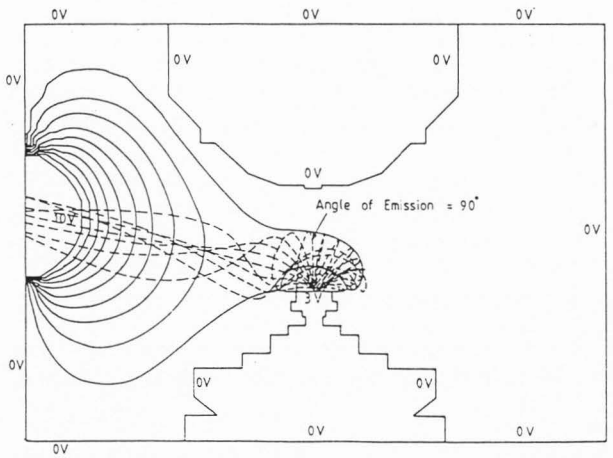

Fig. 5. Application of Algorithm C to electron trajectory tracking in a SEM. (Time Step = $1x10^{-8}$ seconds, Specimen Bias = 3.0 V, Detector Bias = 10 V, Secondary Electron Energy = 2 eV).

the specimen) as the mesh discretisation is fine enough. However, there is still a stray trajectory which is directed towards the top of the figure.

Figs. 5 and 6 show the electron trajectories obtained by algorithm C for a time step of 1 x 10^{-8} s and 5 x 10^{-10} s respectively. The absence of stray trajectories should be noted, indicating that it is a more robust algorithm than either A or B. It is also observed that this algorithm, unlike algorithm A, is not very sensitive to the chosen time step.

Quantitative voltage contrast studies in the SEM

Many studies [8,9,10,15,16,18,36,41,42,43,44,59] have been carried out on the use of voltage contrast as a quantitative voltage measurement technique in the SEM. The main problem limiting the accuracy of this technique is the presence of local fields which arise from the spatially varying potentials and the finite size of the specimen conductors.

Local fields have been classified into type I and type II by various researchers [8,9,10,18,43,44,59]. Type I local field effect (or intra effect) arises from the variation in the voltage at the measurement point itself while type II local field effect (or inter effect) is caused by the voltage variation at the neighbouring electrodes. Type I local field effect will give rise to linearisation error while type II local field effect will cause an error known as false voltage in quantitative voltage contrast measurements.

Most studies on quantitative voltage contrast have however usually simulated and measured these effects using a particular combination of specimen and analyser design. The results obtained are therefore only applicable to that particular analyser-specimen configuration. We have adopted the approach of isolating individually and quantifying the various error voltage components through computer simulation studies using the previously described SE trajectory tracking algorithm. This information is necessary for a systematic approach to the design of low error voltage energy analysers. The results of these studies have been previously reported in [8,9].

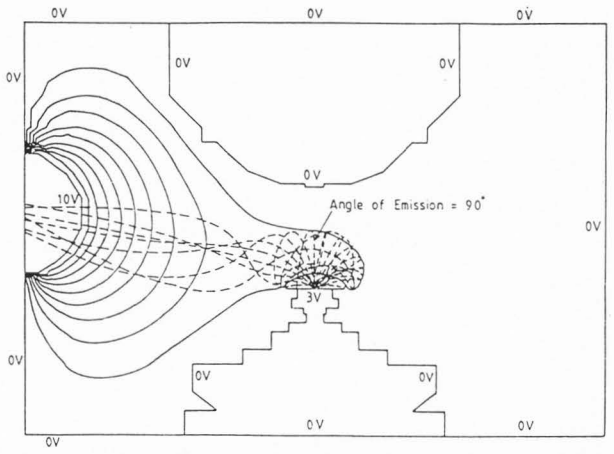

Fig. 6. Application of Algorithm C to electron trajectory tracking in a SEM. (Time Step = $5x10^{-10}$ seconds, Specimen Bias = 3.0 V, Detector Bias = 10 V, Secondary Electron Energy = 2 eV)

SEM Cathodoluminescence

Background

When the high-energy primary electron beam of the SEM impinges on a semiconductor, electron-hole (e-h) pairs are generated in the vicinity of the point of impact. These e-h pairs diffuse away from the point of generation and can recombine, either radiatively or non-radiatively. In the case of radiative recombination, as in III-V semiconductor materials, photons are generated within the semiconductor and propagate in all directions. But only a fraction of these photons emerges from the surface, giving rise to light emission known as cathodoluminescence or CL in short.

To facilitate the quantification of CL signals in the SEM, a theoretical simulation model is required. This model should, among other things, allow one to estimate the generation efficiency and escape probability of photons

for any set of electron beam and specimen conditions, and to study the spatial-angular distribution of the CL signal.

Past theoretical models which have been proposed [23,25,32,51] suffer from the following main drawbacks:

a) The lack of accuracy in treating the electron beam-specimen interaction process in the semiconductor. The electron-hole generation volume is normally represented by either a point or spherical source, or a modified Gaussian approximation. As pointed out by Yacobi and Holt [68], developments of quantitative CL should also involve Monte Carlo calculation of the generation of excess carriers. Hence, a more realistic approach is through Monte Carlo simulation, which accurately describes electron beam scattering within the semiconductor and improves the calculated results for short diffusion lengths [38] especially with high electron beam voltages;

b) The models are limited to treating normal electron beam incidence;

c) In most cases, total interHxl reflection and Fresnel loss [57] of photons at the surface are treated in a very simplified way or ignored.

This section describes an improved three-dimensional model for simulating cathodoluminescence in a semiconductor under electron beam irradiation. The Monte Carlo method is used to simulate the electron beam-semiconductor interaction while Berz and Kuiken's [3] formulation is used to obtain the excess carrier distribution. Optical losses of photons both within the semiconductor and at the semiconductor-air interface are also accounted for in this model. This model has been used to simulate the CL intensity as a function of electron beam voltage, beam incidence angle, surface recombination velocity, diffusion length, absorption coefficient and surface dead layer thickness. The radiation patterns over the top face of specimen with flat geometry have also been simulated.

Monte Carlo simulation

The geometrical configuration of the Monte Carlo calculation is schematically shown in Fig. 7. The situation where the electron beam of the SEM is focussed at an incident angle, Θ_o, on the specimen surface at the origin is considered. The sample is assumed to be semi-infinite, bounded only by the top surface and is divided into many small cubes with dimensions δx, δy and δz at depth h. The top surface is assumed to have a dead layer with a thickness Z_m [67] which has the same properties as the bulk semiconductor as far as beam-specimen interaction is concerned, but in which recombination is mainly through non-radiative centres and therefore non-luminescent in nature.

The Monte Carlo procedure is based on the single-scattering theory of Hawryluk et. al. [22]. The formulation of the model used in this work follows that of Phang [49]. In this approach, each electron is assumed to suffer a number of collisions within the solid, and each

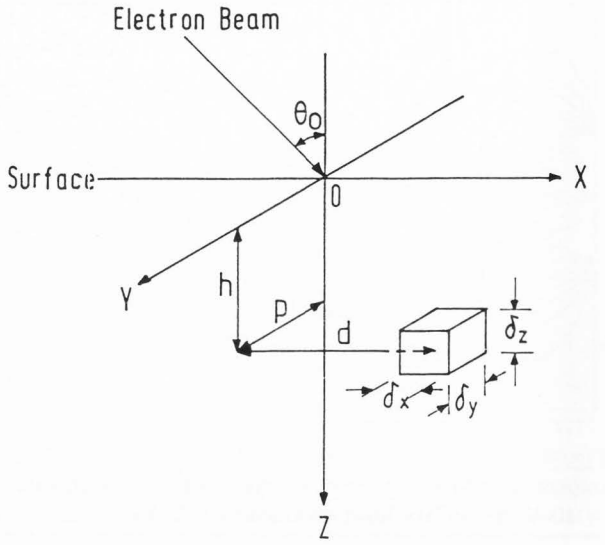

Fig. 7. Physical Model for simulating the beam-material interaction. An electron beam incident at an angle Θ_o on a semi-infinite semiconductor plane which is divided into volume elements for the determination of the spatial distribution of absorbed energy.

scattering event is simulated by calculating, using randomly generated numbers, the angle of deflection, the azimuthal angle and the step length. The energy loss of electrons due to each scattering event is calculated according to the continuous-slowing-down-approximation of Bethe [4], and recorded in the elementary volume in the sample where it occurs. The trajectory of each electron is tracked until the electron has either lost almost all its energy or has been reflected from the solid, i.e. backscattered. The spatial energy dissipation, δE, of all electrons traversing a particular volume is calculated and stored as a matrix of δE versus x, y and z.

Carrier generation and distribution

Due to the small values chosen for δx, δy and δz, each cube in Fig. 7 can be treated as a point source located at the centre of that volume. The generation efficiency of e-h pairs of each source is

$$N_{e\text{-}h} = \delta E / E_{ave} \qquad (17)$$

where E_{ave} is the average energy required for the formation of a single e-h pair and assumed to be about three times the bandgap energy of the semiconductor material. E_{ave} for GaAs is assumed to be 4.5 eV [45].

Van Roosbroeck has developed a general method for evaluating the distribution of excess carriers in the presence of finite surface recombination [60]. However, he has applied the formulation only in the case when the generation source is at the surface. Berz and Kuiken [3] have further analysed in detail this formulation for a finite volume under the surface where the generation of excess carriers actually occurs. Assuming that the sample is a semi-infinite n-type

semiconductor, the appropriate minority carrier differential equation for the injected hole concentration at steady state [3] is

$$D\nabla^2(\delta p) - \frac{\delta p}{\tau} + g = 0 \qquad (18)$$

where g is the generation rate of e-h pairs per unit volume, D is the minority carrier diffusion constant and t is the minority carrier lifetime. The boundary condition at the top surface, z = 0, is

$$Dd(\delta p)/dz = v_s \delta p \qquad (19)$$

where v_s is the surface recombination velocity.

Berz and Kuiken solved eqns. (18) and (19) by assuming that the generation of carriers by the electron beam occurs uniformly within a sphere of radius a, whose centre is at a distance h from the surface as shown in Fig. 8. Let $p_c(r)$ be the density of the excess minority carriers at a distance r from the centre of the sphere. The solution of eqn. (18) for $a << L$ and $r > a$ is [3]

$$p_c(r) = (G\tau/4\pi L^3)\exp(-r/L)/(r/L) \qquad (20)$$

and where G, in e-h pairs/sec, is the total generation rate within the sphere.

Using the method of images and using an analogy in electrostatics, it follows that for the case of zero and infinite surface recombination velocity, the solutions of excess minority carrier concentration are [3]

$$\delta p(x,y,z) = p_c(r) + p_c(r') \qquad (21)$$

$$\delta p(x,y,z) = p_c(r) - p_c(r') \qquad (22)$$

respectively, where $p_c(r)$ and $p_c(r')$ are the excess minority carrier density from the original and its surface image respectively.

For a finite surface recombination velocity, the surface image has the same characteristics as the original source, and a line image that acts as a sink is added (Fig. 8). Using the sources and sink described above and in Fig. 8, the excess minority carrier concentration becomes [3]

$$\delta p(x,y,z) = p_c(r) + p_c(r') - p_1 \qquad (23)$$

for

$$p_1 = \frac{G\tau v_s}{2\pi L^3 D} \int_o^\infty \frac{\exp(-\frac{v_s}{D}q)\,\exp(-r_q/L)}{r_q/L} dq \qquad (24)$$

where

$$r_q = \sqrt{[(d-x)^2+(p-y)^2+(z+h+q)^2]} \qquad (25)$$

This r_q has been modified to account for the contribution of the y-coordinate of the source located at P(d,p,h).

Eqns. (20)-(25) were derived for the case of uniform spherical generation volume. However, Berz and Kuiken have shown that these equations can be valid for a situation of arbitrary distribution extending over a region with dimensions much smaller than L, provided one takes [3]

$$G = \iiint g(x,y,z)\,dx\,dy\,dz \qquad (26)$$

$$\text{and} \quad h = \iiint z\,g(x,y,z)/G\,dx\,dy\,dz \qquad (27)$$

where z is the distance from the surface.

By dividing the generation volume obtained using the Monte Carlo method into small elements with dimensions which are much smaller than L, eqns. (21)-(23) can be readily applied if G and h are now calculated using eqns. (26) and (27) respectively for each small region. The generation rate G in eqn. (26) is determined by referring back to eqn. (17) and is assumed to be zero for the point sources which are outside the generated volume defined by the Monte Carlo method.

The steady state excess minority carrier concentration at any point P(x,y,z) in the semiconductor due to each point source is calculated and the cumulative effects at P(x,y,z) of all the point sources that make up the total generation volume will give the total excess carrier density generated by the electron beam at that point. To account for the dead layer effect near the surface, all the distributed excess minority carriers in the dead layer region are assumed to recombine non-radiatively, giving zero light emission.

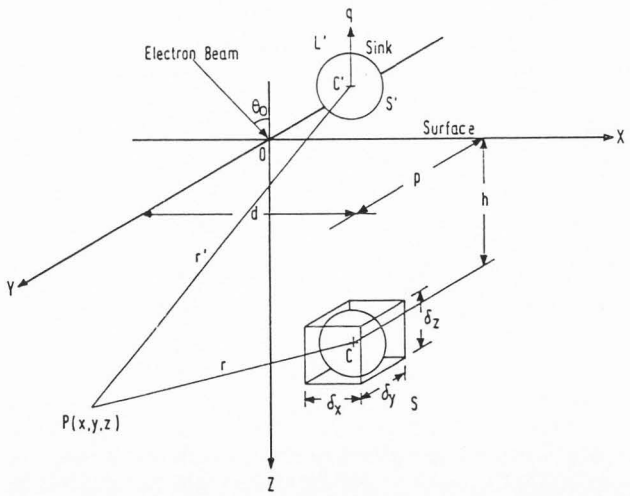

Fig. 8. The method of images for calculating the excess minority carrier density distribution. C and C' are the centres of the generation sphere, S, and its surface image, S', respectively. For $V_s = 0$, S and S' are sources. For $V_s = \infty$, S and S' form a dipole. L' is a line sink introduced to account for the finite surface recombination velocity along the surface. Each elementary volume, size δx by δy by δz, given by the Monte Carlo simulation corresponds to the function g(x,y,z) of eqn. (26).

Optical radiation

The cathodoluminescence emission intensity from the GaAs surface can be calculated from the excess minority carrier density concentration. Photons are generated within GaAs when the excess carriers recombine radiatively. It is assumed that the luminescent intensity of light produced by radiative recombination at a volume element is proportional to the integral of the density of excess carriers over its volume [23] minus the optical losses. It is also assumed that

a) The direction of light propagation from the generation sites, which are also the centres of the small cubes, is isotropic i.e. radiation propagates uniformly in all directions;
b) Light which undergoes more than one internal reflection at the top surface is assumed to have been absorbed by the substrate;
c) In the absence of defects, the bulk recombination of an excess pair of minority carriers is equivalent to the creation of a photon of visible or near-infrared radiation at the recombination site; and
d) The reabsorption of photons within the material is assumed to have negligible effect on carrier transport [61]. This is true for n-type GaAs if the doping does not exceed $10^{18}cm^{-3}$ and for p-type even at higher doping levels.

The three main optical loss mechanisms are [57]: total internal reflection, absorption within GaAs, and Fresnel loss. The first loss mechanism occurs when photons are incident on the surface at angles greater than the critical angle Θ_c, defined by Snell's law,

$$\Theta_c = \mathrm{Sin}^{-1}(n_1/n_2) \tag{28}$$

where $n_2 > 1$ and n_1 are the refractive indices of the incident and refractive sides of the surface respectively. For GaAs, the critical angle is about 16° [57].

For photons propagating towards the surface, the attenuation is given by an exponential law [2],

$$F(\bar{d}) = \exp(-\alpha \bar{d}) \tag{29}$$

with α being the absorption coefficient of the material and $\bar{d}$ the appropriate optical path length that the photons must travel through the semiconductor to reach the top surface.

Although photons incident on the surface at angles greater than Θ_c are internally reflected, those reaching the surface within the critical angle may still be reflected as described by the Fresnel formula [62]. The average transmissivity for an isotropic radiation with random polarisation is [56]

$$T_{av}(x1,x2,n) = \frac{\int_{x1}^{x2} \left[\frac{1}{2} T_s(x,n) + \frac{1}{2} T_p(x,n) \right] dx}{\int_{x1}^{x2} dx} \tag{30}$$

where $n = n_1/n_2$, and T_s and T_p are the transmissivities for radiation whose electric vectors are perpendicular and parallel to the plane of incidence.

For a radiation whose direction of incidence, Θ_i is specified, the transmissivities are given by [38] :

$$T_s(x,n) = 4(1-x)^{1/2}(n^2-x)^{1/2}[(1-x)^{1/2}+(n^2-x)^{1/2}]^{-2} \tag{31a}$$

$$T_p(x,n) = 4n^2(1-x)^{1/2}(n^2-x)^{1/2}[n^2(1-x)^{1/2}+(n^2-x)^{1/2}]^{-2} \tag{31b}$$

where the dependence on the angle of incidence is contained in $x = \sin^2\Theta_i$.

Although eqns. (30) and (31) are derived for $n > 1$, Stern [56] has shown that, for $n < 1$

$$T_{av}(x_1,x_2,n) = n^2\, T_{av}(x_1,x_2,1/n) \tag{32}$$

We have calculated $T_{av}(x_1,x_2,n)$ for different discrete incidence angles with $x_1 = \sin^2\Theta_{i1}$, $x_2 = \sin^2\Theta_{i2}$ where $\Theta_{i2} = \Theta_{i1} + \delta\Theta$. If $\delta\Theta$ is made to be very small, then the discrete T_{av} between Θ_{i1} and Θ_{i2} can be assumed to be constant.

The total loss for radiation which is not totally internally reflected is therefore

$$n_{ex} = F(\bar{d}) * T_{av}(x_1,x_2,n) \tag{33}$$

Eqns. (28)-(33) were used to determine the probability of a ray generated within the bulk of GaAs emerging from the surface as follows. Assuming that photons emitted in GaAs at a depth z propagate uniformly in all direction, only those propagating within the solid angle Θ_c can escape from the surface without suffering total internal reflection. Since the propagation of the luminescence is restricted to just one reflection and Θ_i is known, the optical path distance $\bar{d}$ of eqn. (29) for a particular ray becomes

$$\bar{d} = z / \mathrm{Cos}\Theta_i \tag{34}$$

The partial discrete transmission of the luminescence with $\Theta_{i1} \le \Theta_i \le \Theta_{i2}$ at the interface is given by eqns. (30)-(32). Hence the total attenuation of a ray is, therefore, calculated using eqn. (33).

The net CL emission from the surface is obtained by considering each angle of light propagation from a particular position in the GaAs material and summing up the total contributions. This calculation is then performed for each position at which significant excess carriers are present.

The computation steps for the whole model can be summarised as follows: the Monte Carlo method is used to compute the electron-hole pair generation volume arising from the incident electron beam; the resulting excess carrier distribution is obtained using Berz and Kuiken's formulation of the diffusion equation, and the total light emission is obtained by modelling the optical losses using eqns. (28) - (34).

Results and discussion

This section gives examples of some results which can be obtained from the Cathodoluminescence simulation model presented above.

Emission efficiency, escape probability and emission pattern: Emission efficiency is defined as the ratio of the total number of photons emitted per second from the sample surface to the total number of photons generated per second from all positions in the sample. Fig. 9 shows the variation of emission efficiency of CL light as a function of beam voltage, surface recombination velocity and absorption coefficient for a GaAs sample. The curves show that only a very small amount of light is being transmitted on the first pass from the GaAs to the air. The reduction in emission efficiency for curves 3-6 with increasing electron beam voltage is the result of the internal self-absorption effect. The location at which the maximum excess minority carrier generation occurs moves deeper with rising electron beam voltage, resulting in an increased optical path length between the CL signal formation point and the surface. Since the internal optical absorption is exponentially dependent upon the optical path length and absorption coefficient, an increase in the electron beam energy reduces the probability of photons reaching the top surface, resulting in a fall in CL emission efficiency. It can also be noted by comparing curves 1, 3 and 5, or 2, 4 and 6 in Fig. 9, that an increase in the absorption coefficient reduces the CL signal. The effect of an increasing surface recombination velocity, however, depends on the beam energy and absorption coefficient. At a low absorption coefficient, (cf. curves 1 and 2) V_s has virtually no effect. This is because even the part of the light that is generated at large depths can still be emitted with little self-absorption. When the absorption coefficient is high (cf. curves 5 and 6), only light generated near the surface can be emitted and CL emission becomes very sensitive to surface recombination effects.

Fig. 10 illustrates the dependence of optical loss of photons on the depth of photon generation. The escape probability is here defined as the average probability of photons generated per second from all the luminescent sources in a thin layer at a depth z, arriving at the top semiconductor-air interface and subsequently leaving the surface. It is evident that the exponential attenuation of the GaAs self-absorption can cause a severe drop in the escape probability even with a moderate value of the absorption coefficient. For example, in Fig. 10, the probability drops by 30% at a depth of 3.5 μm from the top surface with α = 0.1 μm^{-1} and to about 0.58% at a depth of 8 μm. From the perspective of improving escape probability, excess carrier generation at shallow depths would be preferable. However, this can only be achieved by either using low electron beam voltages or by tilting the sample at an angle to the incident electron beam and both would result in very low excess carrier generation and high surface recombination.

Fig. 11 shows the typical CL emission pattern or angular distribution over a flat GaAs sample. The electron beam voltage is set at 25 kV with the beam incidence angle, Θ_o= 0°. The other important parameters are L=2.0 μm, Z_m= 0, and the normalised surface recombination velocity V_s is infinite. The normalised surface recombination velocity is defined here as $V_s = v_s\sqrt{(\tau/D)}$. In the figure, n_1 is assumed to have a value of 1 while n_2=3.66, which is the case for GaAs. The CL intensity is plotted as a function of the angle of refraction, β_o, and normalised by the intensity in the direction of the normal to the surface. The plot, which gives the normalised CL intensity angular distribution for two extreme values of the absorption coefficient α, shows that α does not significantly influence the polar radiation in GaAs. The CL radiation pattern for a GaAs surface is close to a cosine distribution.

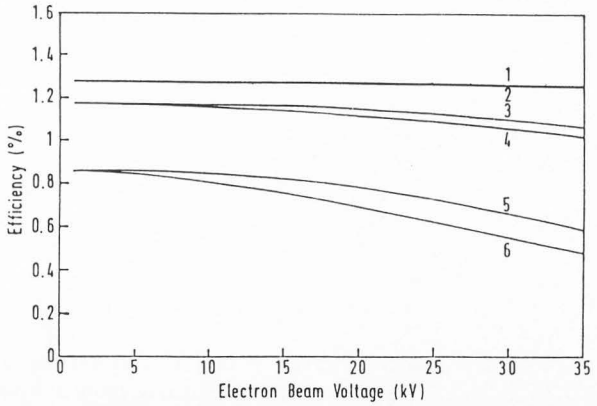

Fig. 9. Emission efficiency for the first pass photons at different values of absorption coefficients and the two extreme values of V_s. (1) V_s = 0, α = 0.01 μm^{-1} (2) V_s = 50, α = 0.01 μm^{-1} (3) V_s = 0, α = 0.1 μm^{-1} (4) V_s = 50, α = 0.1 μm^{-1} (5) V_s = 0, α = 0.5 μm^{-1} (6) V_s = 50, α = 0.5 μm^{-1}. The efficiency takes account of the three optical loss mechanisms. Other relevant parameters are set at L = 1.00 μm, Z_m = 0, Θ_o = 0°.

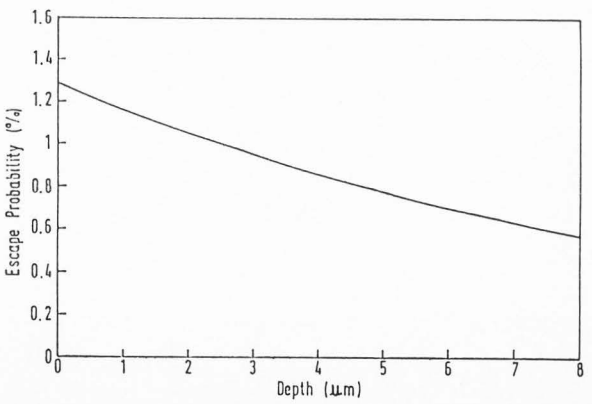

Fig. 10. Escape probability of CL photons generated at different depths. Relevant parameters are beam energy of 30 kV, V_s = 50, L = 1.0 μm, α = 0.1 μm^{-1}, Zm = 0, Θ_o = 0°.

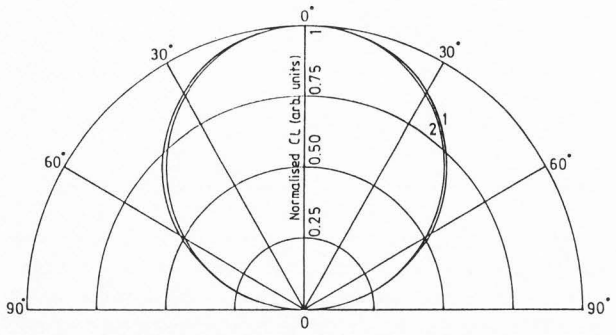

Fig. 11. Polar plot of normalised CL intensity radiation patterns for two extreme values of α. (1) α = 0.01 μm^{-1} and (2) α = 1.0 μm^{-1}. Material is GaAs with other relevant parameters set at 25 kV, L = 2.00 μm, Zm = 0, $V_s = \infty$ and $\Theta_o = 0°$.

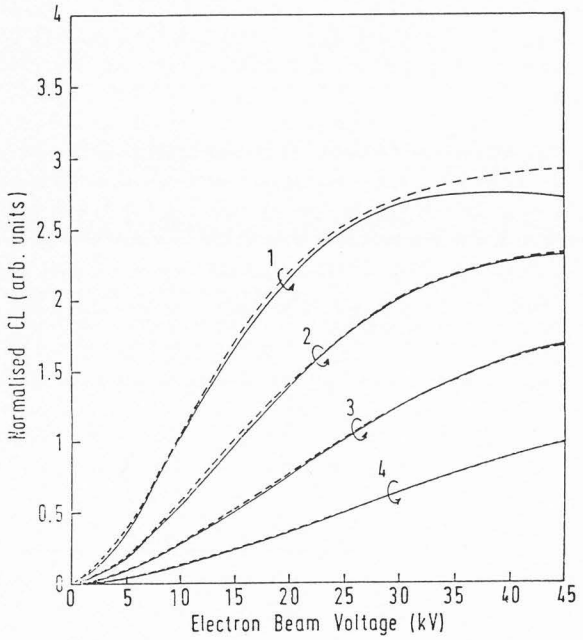

Fig. 12. Effect of the diffusion length on the normalised CL signal in GaAs. (1) L = 0.5 μm (2) L = 1 μm (3) L = 2 μm (4) L = 4 μm. Other parameters are α = 0.1 μm^{-1}, $V_s = \infty$, Zm = 0, $\Theta_o = 0°$. Solid line by the present model, broken line by Hergert et al's [14] model.

Influence of semiconductor parameters on CL emission: The simulation model has also been used to study the effects of various material parameters, particularly surface recombination velocity, diffusion length, optical absorption coefficient and dead layer thickness, on the CL signal intensity. Results of this study have revealed that the relationship between semiconductor parameters and the CL signal is complex and generally non-linear. Some examples are given below.

The dependence of the CL signal on the diffusion length and the absorption coefficient are plotted in Figs. 12 and 13

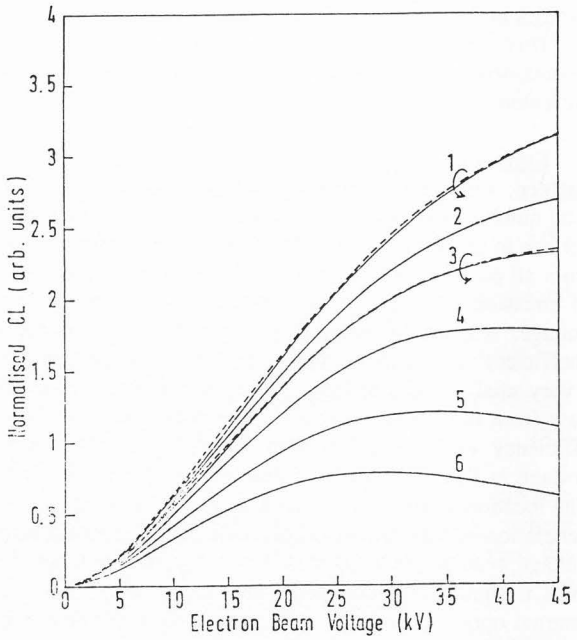

Fig. 13. Effect of the absorption coefficient on the normalised CL signal in GaAs. (1) α = 0 μm^{-1} (2) α = 0.05 μm^{-1} (3) α = 0.1 μm^{-1} (4) α = 0.2 μm^{-1} (5) α = 0.4 μm^{-1} (6) α = 0.7 μm-1. Other parameters are L = 1.0 μm, $V_s = \infty$, Zm = 0, $\Theta_o = 0°$. Solid line by the present model, broken line by Hergert et al's [14] model.

respectively. Fig. 12 indicates that CL intensity decreases with increasing diffusion length. This is due to the increased spreading of excess carriers. In one direction, diffusion towards the surface results in more non-radiative surface recombination. Diffusion in the other direction deeper into the bulk results in CL emission which has to propagate a longer distance to reach the surface, thus resulting in larger self-absorption losses. It is therefore reasonable to expect the CL intensity to decrease with increasing diffusion length.

Self-absorption also accounts for the maximum observed in the dependence of CL emission with beam energy in the case of L=0.5 μm. The higher beam energies result in electron-hole pairs and CL emission taking place deeper beneath the surface. For the same reason, a maximum is also present in curves 5 and 6 of Fig. 13 in which α = 0.4 μm^{-1} and 0.7 μm^{-1} respectively at a diffusion length of 1.0 μm.

It can also be observed in Fig. 12 that varying the diffusion length affects the slope of the curve more at lower beam energies than at higher beam energies. This can be explained by the relatively shallow depth and small interaction volume of the beam electrons. Distribution of the steady state excess carrier can be significantly affected by changes in the diffusion length. At high beam energies, the interaction volume is fairly large and deep, and variations in the diffusion length will not have such a large effect on the steady state excess carrier distribution and

therefore the CL emission. However, it can be seen in Fig. 13 that the absorption coefficient affects the CL dependence on beam energy principally at high beam energies. This is because at high energies, where most of the excess carriers and therefore the CL emission sites are deeper below the surface, the amount of light which can leave the material surface is very sensitive to the rate of absorption as it propagates towards the surface. Thus, the CL emission versus beam energy curve is heavily dependent on the material diffusion length at low energies and on material absorption coefficient at high energies. This phenomenon can provide interesting possibilities in the determination of these material parameters. Results of Hergert et. al.'s model [24] are also plotted alongside our simulated results in Figs. 12 and 13, and it can be observed that they are in good qualitative agreement.

Indirect Charging Of Specimens in the SEM

Background

In the scanning electron microscope (SEM), when primary electrons (PE) impinge on the specimen, both secondary electrons (SE) and backscattered electrons (BSE) are generated. In subsequent discussion, the entire spectrum of generated electrons will be collectively known as 2Es.

The 2Es can impinge on other parts of the specimen and generate another spectrum of electrons, the latter will be known as 3Es. In fact, the scintillator-photomultiplier detector of the SEM is not able to distinguish the 2Es and 3Es; thus the classification here is only for convenience of presentation. The 3Es can also generate subsequent spectra of electrons, and the process continues.

Electron-solid interaction can be summarised in one simple equation

$$I_{PE} = I_2 + I_{sp} \tag{35}$$

where I_{PE} is the primary beam current, I_2 is the emitted 2Es current (i.e. $I_{SE} + I_{BSE}$) and I_{sp} is the specimen current.

The ratio of I_2 to I_{PE} is called the emission yield ($Y_2 = I_2/I_{PE}$). For most materials, there are two crossover points at which the yield is unity, i.e. the generated 2Es current equals to the impinging PE current. These two crossovers are called E_{P1} and E_{P2}, where $E_{P2} > E_{P1}$. Below E_{P1}, and above E_{P2} the electron yield is less than unity. Between E_{P1} and E_{P2}, the yield is greater than one.

When the yield is greater than one, the generated current (I_2) is greater than primary current (I_{PE}), and as a result, the specimen is depleted of electrons. On the other hand, when the yield is less than one, the generated current (I_2) is less than the impinging current (I_{PE}). As a result, the specimen experiences a net gain of electrons. In both cases, one can say that excess charges (either positive or negative) are generated in the specimen.

If the specimen has a conductive path to either a charge reservoir or sink, the excess charges will always be neutralized and the specimen will remain at its initial potential. However, if no conductive paths exist, these excess charges will accumulate and cause the potential on the specimen to change. Under such a situation, one can say that the specimen is charging-up. Here the charging-up of the specimen due to direct PE irradiation is classified as direct charging.

In some situations, certain portions of the specimen may not be irradiated directly by the primary beam. However, the generated 2Es may still impinge on these parts of the specimen. If these parts are electrically floating, it is very likely that they will gain or lose charges causing the specimen to charge up negatively or positively. The charging up of specimens by secondary (2Es) or tertiary (3Es) irradiation is known as indirect charging. Fig. 14 depicts a practical situation of indirect charging which one will encounter in electron-beam testing of integrated circuits. In this set-up, the die sits in a epoxy or ceramic cavity. The insulator wall is not coated with a conductive coating and thus will charge up under 2Es irradiation.

Specimen charging generates external electric field around the specimen. A weak external field causes commonly observable behaviours like the deflection of the low energy SEs, bright areas due to the increased emission of electrons as a result of repulsion by the negatively-charged specimen surface, dark areas due to attraction of SEs by the positive surface charges. Strong external fields can deflect the PE away and distorted the raster scan image [20,28,55]. Specimen charging can introduce significant errors in quantitative SEM work such as critical dimension measurements [6], voltage measurements [46] and electron-beam lithography [14,31]. On the positive side, specimen charging can be used for the testing of PCB boards [7].

Specimen charging can be eliminated by application of a conductive coating. In certain applications, conductive coatings may not be possible. In these situations, the specimen charging can be minimised or even eliminated by

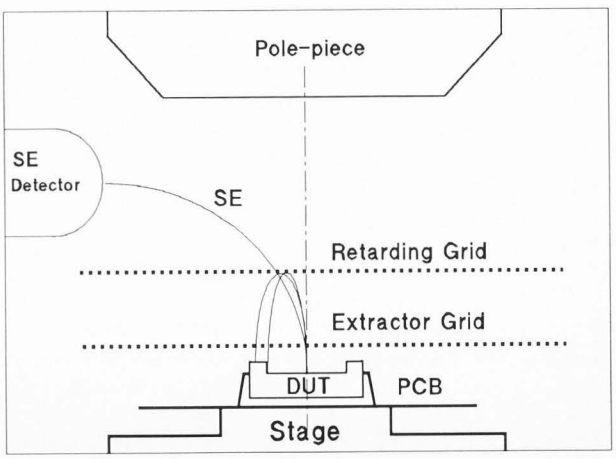

Fig. 14. Schematic diagram (not to scale) showing the measurement set-up for electron beam testing of integrated circuits in SEM. The die is sitting in the ceramic package cavity. The cavity wall is not exposed to the primary electron, nevertheless, it can charge up due to bombardments by secondary electrons and backscattered electrons emitted from the die.

various charge neutralization schemes [13,20] and operation of the SEM under certain beam conditions [34,66].

This section presents a simulation model to study the dynamics of indirect charging on the specimen structure shown in Fig. 14.

Solution of a self-consistent electric field

The electric field distribution of the physical system is fully described by Poisson's equation and the imposed boundary conditions. Solution of this equation with the imposed boundary conditions yield the self-consistent electric field in the entire simulation domain. A two-dimensional (2-D) cartesian model is used in this simulation. The simulation domain is discretised into many small piecewise linear elements (called finite elements) to facilitate the solution of Poisson's equation and trajectory tracking of the moving and trapped charges.

Representation of time, charges and material properties

Consider the case where beam energy is E_{PE} = 1 keV and beam current is I_{PE} = 1 nA. After leaving the extraction grid, the PE takes approximately t = 530 ps to reach the specimen (the IC package is about 10 mm below the extraction grid). In this time frame, there are approximately less than 10 PEs making their way to the specimen target. There may be some few tens of 2Es leaving the specimen. Thus there will be less than a hundred moving electrons in this time frame. The moving electron density is so low that one can ignore the interactions among the moving particles. In solving Poisson's equation, one can safely ignore the moving charge density. Since there are no interactions among the moving charges, all the PEs in any time interval T_{ex} ($T_{ex} >> t$) can be represented by a super-particle of energy E_{PE} carrying a charge $I_{PE}T_{ex}$. This time interval T_{ex} is defined as the PE exposure time.

In this model, the specimen target is aluminium while the cavity wall is made of ceramic. The measured SE and BSE yield data of these two materials are stored in a look-up table. When a super particle with energy E impinges on the material M at an impact angle θ, the SE and BSE yields obtained from the look-up table are: $Y_{SE}(M, E, \theta)$ and $Y_{BSE}(M, E, \theta)$. The generated SE and BSE have a specific normalized energy distribution given by $G_{SE}(M, E)$ and $G_{BSE}(M, E)$. Both SE and BSE are assumed to be emitted into a cosine distribution regardless of the incoming electron energy and impact angle.

To save on computational time and storage space, the energy spectrums are discretised into distinct bands. All 2Es in a particular band will be considered to have energy E_j, where E_j is the average energy of band j. Similarly, the angular distribution is also discretised into distinct angular sectors; all 2Es falling in that particular sector k will be represented by angle θ_k. In this way, each energy and angular spectrum combination will be represented by one super-particle having initial energy E_j and emission angle θ_k. The charge carried by each super particle is the product of the areas in band j and sector k.

From the initial energy and emission angle, the x and y component of the super-particle velocity (V_x, V_y) are calculated. The electron emission point is taken to be at the impinging point. This pair of initial conditions, i.e. position (x, y) and velocity (V_x, V_y), fully characterize the emitted 2Es. These initial conditions are then loaded into a set of arrays containing similar information for all other travelling electrons.

Tracking of electron trajectories

In this simulation model, first-order linear finite elements are used in the solution of Poisson's equation. In this type of element, the potential is continuous everywhere in each element and piece-wise continuous across elements. As a result the field is constant in each element and discontinuous across elements. Field discontinuity at the element boundary introduces errors into the numerical calculation of the PE trajectories. The PE trajectories can be observed to perform a "zig-zag" motion across the element boundaries.

To overcome this problem, a bi-cubic Hermite interpolation scheme [21,37] is used to interpolate the element potentials (given the nodal potential values). In the interpolation scheme, the dependent variable (i.e. the potential) and its derivative (i.e. the field) is continuous everywhere in the simulation domain. The second derivative of potential is piece-wise continuous across elements. This interpolation scheme provides a very smooth field for trajectory tracking of the PEs. A Runge-Kutta routine is used to integrate the equations of motion.

Once the emitted 2Es are grouped into super particles, their subsequent status (i.e. position and velocity) in the electric field are tracked by the trajectory tracking algorithm (algorithm C) detailed in the section on "A secondary electron tracking algorithm". This scheme only requires one past history of the trajectory and is computationally very fast, efficient, moderately accurate and simple to implement.

Treatment of excess charges in electrically floating specimens

The interaction of the PE with the specimen and the subsequent generation of 2Es produced excess charges in the target. In this simulation model, the specimen target (a conductor) is assumed to be connected to some electron source or sink. As a result, there is no accumulation of excess charges in the target and no direct charging of the target specimen.

Interaction of the 2Es with the floating specimen, however, leaves behind some excess charges. These excess charges charge up the floating specimen. This section describes the treatment of these excess charges on insulator specimens.

When excess charges are generated in the insulator, they remain at the point where they were generated, and as a result, a localized surface charge density is produced on the insulator surface. The generated excess charges are assigned to the grid points using the Particle-In-Cell (PIC) scheme [5] (i.e. the nodal charge density). This nodal charge density is updated at the end of each PE exposure time step T. With this, the potential inside and outside the insulator can be obtained by the solution of Poisson's equation with the imposed boundary conditions. The excess charge density

can have a significant effect on the trajectories of travelling super particles, and thus the PE exposure step, T must not be too long.

Immobile localized nodal charge density produces field density gradients within the insulator itself and also between the insulator and the nearby conductors. When the field gradient within the insulator surface reaches a certain critical value, the conduction process can take place and the local charge density gradient is reduced. Similarly, when the field gradient between the insulator surface and the nearby conductor exceeds the breakdown threshold of the vacuum, discharge takes place which reduces the charge density on the insulator surface. These discharge processes, however, are not included in the model.

Results

Fig. 15 shows a series of contour plots of the potential distribution of the specimen structure in Fig. 14 as a function of the beam exposure time. The PE exposure time step is 2.5 seconds, beam current is 1 nA and beam energy is 1 keV. In this simulation, the cavity wall is not exposed to the primary electrons. The cavity wall charges up positively due to bombardment by secondary and backscattered electrons from the target.

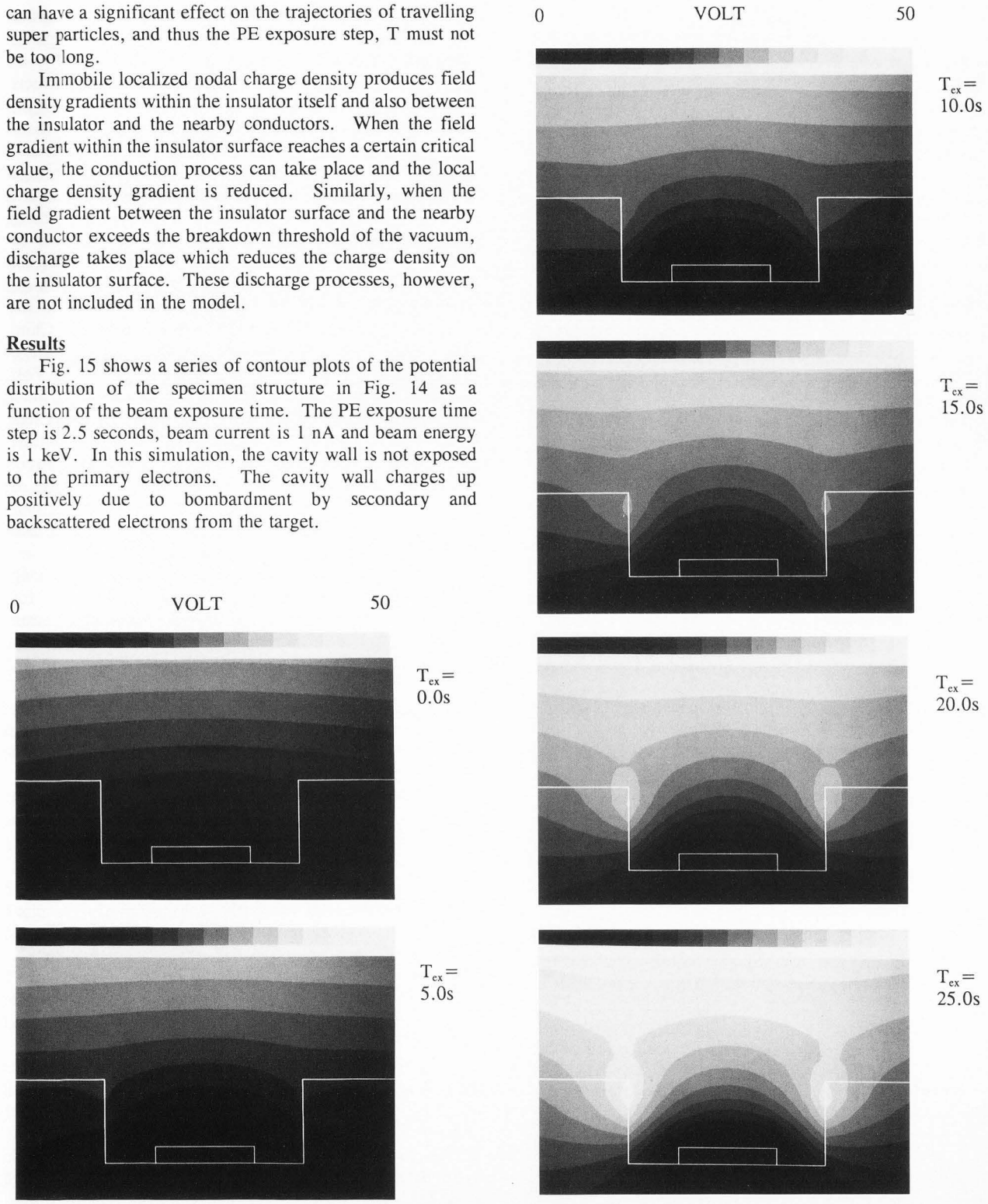

Fig. 15. Series of equipotential plots showing the charging up of the insulator cavity with beam exposure time. The primary beam energy is 1 keV and the beam current is 1 nA. The primary beam exposure time step (T_{EX}) is 2.5 seconds, only alternate frame of potential plots are shown. The cavity is 8 mm wide and 2 mm deep. Extraction grid is 10 mm above the IC package and is held at 100 volts. On the plot, the minimum voltage is 0 volt and the maximum voltage is 50 volt. The voltage range is divided into 16 linear bands as shown on top of each plot.

Conclusion

Simulation models for quantifying three electron beam induced phenomena, namely voltage contrast, cathodoluminescence and indirect specimen charging, are presented. The voltage contrast model comprises a electric field computation program using the finite-element approach and a secondary electron trajectory tracking algorithm. This tracking algorithm employs a linear variation of the electric field within each mesh, which is more accurate than the conventional electron trajectory tracking algorithms using the constant electric field assumption between electron transitions. Using this model, results of qualitative voltage contrast effects on secondary electron trajectories in the specimen chamber of the scanning electron microscope (SEM) are shown. This model can also be used for quantitative voltage studies for designing low error voltage energy analysers.

The cathodoluminescence (CL) model consists of programs for simulating the electron beam-specimen interaction via Monte Carlo analysis, excess carrier generation and distribution, and optical losses of the CL emission. Results showing the variation of CL intensity as a function of surface recombination velocity, diffusion length, and absorption coefficient are presented. This model can also be used to study the variation of CL intensity with electron beam voltage, beam incidence angle and surface dead layer thickness.

The indirect specimen charging model uses the finite-element method to solve Poisson's equation. Two different trajectory tracking algorithms are used. Primary electrons are tracked using a high-accuracy algorithm based on Hermite-Cubic interpolation of electric field which is continuous everywhere in the simulation domain. Secondary and backscattered electrons are tracked using the trajectory tracking algorithm based on linearly interpolated fields. Electron-solid interactions are represented by experimentally measured electron yield data. Simulation has shown that the cavity can charge up to either polarity depending on the electron yield of the material under electron-beam bombardment.

References

[1] Balk LJ, Feuerbaum HP, Kubalek E and Menzel E, "Quantitative Voltage Contrast at High Frequencies in the SEM", Scanning Electron Microsc. 1976; IV: 615-624,646.

[2] Bergh AA and Dean PJ, "Light Generation Efficiency and Light-emitting Diode Design", in Light-Emitting Diodes, Ed. by Hammond P and Walsh D, Oxford: Clarendon Press, 1976, pp. 69-294 and 457-521.

[3] Berz F and Kuiken HK, "Theory of Life Time Measurements with the Scanning Electron Microscope: Steady State," Solid-State Electron., Vol. 19, 1976, pp. 437-445.

[4] Bethe HA and Ashkin J, in Experimental Nuclear Physics, Vol. 1, Ed. by Segre E, John Wiley, 1953, pp. 166-357.

[5] Birdsall CK and Langdon AB, "Plasma Physics Via Computer Simulation", McGraw-Hill Book Company, 1985, pp. 305-311.

[6] Brunner M and Schmid R, "Charging Effects in low voltage scanning electron microscope metrology", Scanning Electron Microsc. 1986; II: 377-382.

[7] Brunner M, Kolbenschlag, Westerman G and Lischke B, "Bare-board testing: the charge storage problem", Microelectronic Engineering 8, 1988, pp. 25-35.

[8] Chan DSH, Low TS, Chim WK and Phang JCH, "The Influence of Analyser Geometry Effects in Scanning Electron Microscope Voltage Contrast Measurements", Scanning Microsc., Vol. 2, No. 3, 1988, pp. 1419-1426.

[9] Chan DSH, Low TS, Phang JCH and Chim WK, "Error Voltage Components in Quantitative Voltage Contrast Measurement Systems", Scanning Microsc., Vol. 5, No. 2, 1991, pp. 345-355.

[10] Chim WK, Phang JCH, Low TS and Chan DSH, "An Overview of Quantitative Voltage Contrast Measurements in the Scanning Electron Microscope", Proc. of the Int. Symp. on the Physical and Failure Analysis of ICs, 19-20 Oct 1987, Singapore, IEEE Singapore Section, pp. 14-19. (Obtainable from IEEE Singapore Section, 200 Jalan Sultan, #11-03 Textile Centre, Singapore 0719)

[11] Chim WK, Low TS, Chan DSH and Phang JCH, "Electron Trajectory Tracking Algorithms for Analysing Voltage Contrast Signals in the Scanning Electron Microscope", J. Phys D.: Appl. Phys. 21, 1988, pp. 1-9.

[12] Chin ISH, Chim WK, Koh PCT, Chan DSH, Low TS, Phang JCH and Ho PYS, "Observation of Integrated Circuit Surface Potentials with Voltage Contrast", Proc. of the NUS Symposium on Applications of Scanning Electron Microscopy, 9 Sep 1988, National University of Singapore, pp. 82-87.

[13] Crawford CK, "Ion charge neutralization effects in scanning electron microscopes", Scanning Electron Microsc. 1980; IV: 11-24.

[14] Cummings KD and Kiersh M, "Charging effects from electron beam lithography", J. Vac. Sci. Technol. B, Vol 7(6), 1989, pp. 1536 - 1539.

[15] De Jong JL and Reimer JD, "Effects of Local Fields on Electron Beam Voltage Measurement Accuracy", Scanning Electron Microsc. 1986; III: 933-942.

[16] Dinnis AR, "Detectors for Quantitative Electron Beam Voltage Measurements", Scanning Microsc., Vol. 2, No. 3, 1988, pp. 1407-1418.

[17] Fujioka H, Nakamae K and Ura K, "Function Testing of Bipolar IC's and LSI's with the Stroboscopic Scanning Electron Microscope", IEEE Journal of Solid State Circuits, Vol. SC-15, No. 2, April 1980, pp. 177-183.

[18] Fujioka H, Nakamae K and Ura J, "Local Field Effects on Voltage Measurement using a Retarding Field Analyser in the Scanning Electron Microscope", Scanning Electron Microsc. 1981; I: 323-332.

[19] Gorlich S, Herrmann KD, Reiners W and Kubalek E, "Capacitive Coupling Voltage Contrast", Scanning Electron Microsc. 1986; II: 447-464.

[20] Gressus C le, Vigouroux JP, Duraud JP,

Boiziau C and Geller J, "Charge Neutralization on insulators by electron bombardment", Scanning Electron Microsc. 1984; I: 41-48.

[21] Hawkes P W and Kasper E, "Principles Of Electron Optics, Vol 1: Basic Geometrical Optics", Academic Press, 1989, pp. 188-198.

[22] Hawryluk DJ, Hawryluk AM and Smith HI, "Energy Dissipation in a Thin Polymer Film by Electron Beam Scattering", J. Appl. Phys., Vol. 45, No. 6, 1974, pp. 2551-2566.

[23] Hergert W and Pasemann L, "Theoretical Study of the Information Depth of the Cathodoluminescence Signal in Semiconductor Materials", Phys. Stat. Sol.(a), Vol. 85, 1984, pp. 641-648.

[24] Hergert W, Reck P, Pasemann L and Schreiber J, "Cathodoluminescence Measurements using the Scanning Electron Microscope for the Determination of Semiconductor Parameters", Phys. Stat. Sol.(a), Vol. 101, 1987, pp. 611-618.

[25] Hildebrandt S, Schreiber J, Hergert W and Petrov VI, Determination of the Absorption Coefficient and the Internal Luminescence Spectrum of GaAs and $GaAs_{1-x}P_x$ (x=0.375, 0.78) from Beam Voltage Dependent Measurements of Cathodoluminescence Spectra in the Scanning Electron Microscope", Phys. Stat. Sol. (a), Vol. 110, 1988, pp. 283-291.

[26] Holt DB and Datta S, "The Cathodoluminescence Mode as an Analytical Technique: Its Developments and Prospects", Scanning Electron Microsc. 1980; I: 259-278.

[27] Holt DB and Saba FM, "The Cathodoluminescence Mode of the Scanning Electron Microscope: A Powerful Microcharacterization Technique", Scanning Electron Microsc. 1985; III: 1023-1045.

[28] Ichinokawa T, Hyama M and Onoguchi A, "Charging effect of specimen in scanning electron microscope", Japanese Journal of Applied Physics, Vol 13(8), 1974, pp. 1272 -1277.

[29] Ioannou DE and Dimitriadis C.A., "A SEM-EBIC Minority-Carrier Diffusion-Length Measurement Technique", IEEE Trans. Elec. Dev., Vol. ED-29, No. 3, March 1982, pp. 445-450.

[30] Ioannou DE and Gledhill RJ, "SEM-EBIC and Traveling Light Spot Diffusion Length Measurements: Normally Irradiated Charge-Collecting Diode", IEEE Trans. Elec. Dev., Vol. ED-30, No. 6, June 1983, pp. 577-580.

[31] Itoh H and Nakamura K, "Investigation of charging effects on the SiO_2 layers with the electron beam lithography system", J. Vac. Sci. Technol. B Vol 7(6), 1989, pp. 1532 - 1535.

[32] Jakubowicz A, "Theory of Cathodoluminescence Contrast from Localized Defects in Semiconductors", J. Appl. Phys., Vol. 59, No. 6, 1986, pp. 2205-2209.

[33] Janssen et. al., "High Spatial Resolution Potential Measurements using Secondary Electrons", Surface Science 93, 1980, pp. 453-470.

[34] Joy DC, "Control of charging in low voltage SEM", Scanning, Vol 11, 1989, pp 1-4.

[35] Khursheed A and Dinnis AR, "Computation of Trajectories in Voltage Contrast Detectors", Scanning, Vol. 5, 1, 1983, pp. 25-31.

[36] Khursheed A and Dinnis AR, "A Comparison of Voltage Contrast Detectors", Scanning, Vol. 6, 2, 1984, pp. 85-95.

[37] Khursheed A and Dinnis AR, "High accuracy electron trajectory plotting through finite-element fields", J. Vac. Sci. Technol. B, Vol 7(6), 1989, pp. 1862-1865.

[38] Landau LD and Lifshitz EM, "Electrodynamics of Continuous Media", Addison-Wesley, 1960, Sec. 66.

[39] Leamy HJ, Kimerling LC and Ferris SD, "Electron Beam Induced Current", Scanning Electron Microsc. 1978; I: 717-726.

[40] May TC, Scott GL, Meieran ES, Winer P and Rao VR, "Dynamic Fault Imaging of VLSI Random Logic Devices", IEEE/IRPS 1984, pp. 95-108.

[41] Menzel E and Brunner M, "Secondary Electron Analysers for Voltage Measurements", Scanning Electron Microsc. 1983; 65-75.

[42] Menzel E and Kubalek E, "Secondary Electron Detection Systems for Quantitative Voltage Measurements", Scanning, Vol. 5, 1983, pp. 151-171.

[43] Nakamae K, Fujioka H and Ura J, "Local Field Effects on Voltage Contrast in the Scanning Electron Microscope", J. Phys. D: Appl. Phys., 14, 1981, pp. 1939-1960.

[44] Nakamura H and Sato Y, "An Analysis of the Local Field Effect on Electron Probe Voltage Measurements", Scanning Electron Microsc. 1983; III: 1187-1195.

[45] Newbury DE, Joy DC, Echlin P, Fiori CE and Goldstein JI, in Advanced Scanning Electron Microscopy and X-Ray Microanalysis, Plenum Press, 1986, pp. 45-86.

[46] Nye P and Dinnis A, "Extraction field and oxide charging in voltage contrast systems", Scanning Vol 7, 1985, pp. 117-124.

[47] Oatley CW and Everhart TE, "The Examination of p-n Junctions with the Scanning Electron Microscope", J. Electronics, 2, No. 6, 1957, pp. 568-570.

[48] Pey KL, Chim WK, Phang JCH, Chan DSH and Chong KY, "SEM Cathodoluminescence for Failure Analysis of Optoelectronic Devices", Proc. of the 2nd Int. Symp. on the Physical and Failure Analysis of ICs, Singapore, 7-9 November 1989, pp. 27-32. (Obtainable from IEEE Singapore Section, 200 Jalan Sultan, #11-03 Textile Centre, Singapore 0719)

[49] Phang JCH, in Line Width Control in Electron Beam Lithography, PhD. Dissertation, University of Cambridge, 1979, Ch. 2.

[50] Plows GS and Nixon WC, "Stroboscopic Scanning Microscopy", Journal of Scientific Instruments (Journal of Physics E), Series 2, Volume 1, 1968, pp. 595-600.

[51] Rao-Sahib TS and Wittry DB, "Measurement of Diffusion Lengths in p-type Gallium Arsenide by Electron Beam Excitation", J. Appl. Phys., Vol. 40, No. 9, 1969, pp. 3745-3750.

[52] Reddy JN, "An Introduction to the Finite Element Method", 1st ed., McGraw-Hill, 1985, pp. 194-395.

[53] Schick JD, "Electron Beam Induced Current Analysis of Integrated Circuits", Scanning Electron Microsc. 1981; I: 295-304.

[54] Schick JD, "Advances in Electron Beam Induced Current Analysis of Integrated Circuits", Scanning Electron Microsc. 1985; I: 55-66.

[55] Shaffner TJ and Hearle JWS, "Recent advances in understanding specimen charging", Scanning Electron Microsc. 1976; I: 61-70.

[56] Stern F, "Transmission of Isotropic Radiation across an Interface between Two Dielectrics", Appl. Optics, Vol. 3, No. 1, 1964, pp. 111-113.

[57] Sze SM, "LED and Semiconductor Lasers", in Physics of Semiconductor Devices, 2nd ed., John Wiley & Sons, 1981, pp. 692-695.

[58] Tuma JJ, "Engineering Mathematics Handbook", 2nd ed., McGraw-Hill, pp. 224-225.

[59] Ura K, Fujioka H and Nakamae K, "Reduction of Local Field Effect on Voltage Contrast", Scanning Electron Microsc. 1984; III: 1075-1080.

[60] Van Roosbroeck W, "Injected Current Carrier Transport in a Semi-infinite Semiconductor and the Determination of Lifetimes and Surface Recombination Velocities", J. Appl. Phys., Vol. 26, No. 4, 1955, pp. 380-391.

[61] Von Roos O, "Influence of Radiative Recombination on the Minority-carrier Transport in Direct Band-gap Semiconductors", J. Appl. Phys., Vol. 54, No. 3, 1983, pp. 1390-1398.

[62] Wangsness RK, "Reflection and Refraction of Plane Waves", in Electromagnetic Fields, John Wiley & Sons, 1979, pp. 457-485.

[63] Wardly GA, "Magnetic Contrast in the Scanning Electron Microscope", J. Appl. Phys. 42, 1971, pp. 376-386.

[64] Watanabe M, Actor G and Gatos HC, "Determination of Minority-Carrier Lifetime and Surface Recombination Velocity with High Spatial Resolution", IEEE Trans. Elec. Dev., Vol. ED-24, No. 9, September 1977, pp. 1172-1177.

[65] Wells OC, "Some Theoretical Aspects of Type I Magnetic Contrast in the Scanning Electron Microscope", Journal of Microscopy, Vol. 139, 1985, pp. 187-196.

[66] Werner HW and Warmoltz N, "Beam techniques for analysis of poorly conducting materials", J. Vac. Sci. Technol. A, Vol 2(2), 1984, pp. 726-729.

[67] Wittry DB and Kyser DF, "Measurement of Diffusion Lengths in Direct-gap Semiconductors by Electron Beam Excitation", J. Appl. Phys., Vol. 38, No. 1, 1967, pp. 375-382.

[68] Yacobi BG and Holt DB, "Future Developments in Cathodoluminescence Microscopy of Inorganic Solids", Plenum Press, 1990, pp. 269-271.

[69] Yuan J, Senkel R and Reimer L, "Recording of Magnetic Contrast Type I by Two-Detector System", Scanning, Vol. 9, 1987, pp.249-256.

[70] Zienkiewicz OC, "The Finite Element Method in Engineering Science", McGraw-Hill, 1967, pp. 1-47.

Discussions With Reviewers

AR Dinnis: In discussing Figs. 2 and 3, you state that the accuracy of the trajectory simulation can be judged by the behaviour of the 2 eV electron emitted at 90° to the surface. It is true that in a uniform retarding field, a 2 eV electron would exactly reach the -2V equipotential (relative to the surface) before turning and falling back. However, the field is not uniform and the trajectory is curved so one would not expect the electron to quite reach the -2V equipotential. On the scale used for the diagram, it is difficult to judge which is the more accurate of the simulations in Figs. 2 and 3. Would it therefore be possible to provide an enlarged view of the situation close to the specimen? This would also help to clarify the exact layout of the specimen (at 3 V) in relation to the specimen stub (at 0 V).

Authors: For electrons which do reach a certain equipotential line, conservation of energy must hold, i.e. a 2 eV electron would be turned back once it reaches the -2 V equipotential line (relative to the surface) irregardless of the uniformity of the retarding field. A more extensive investigation of the relative accuracies of the three algorithms has been reported in reference [11] (Chim WK et. al., J. Phys. D.: Appl. Phys. 21, 1988, pp. 1-9), by comparing the electron trajectories moving under the influence of the electric field generated by an infinitely long wire. The results of the simulation in [11] showed that algorithm C (the linear electric field approach) is the most accurate and also the most robust of the three algorithms with regards to insensitivity to the chosen time step and mesh size. In answer to the second part of the question, the field around the 3 V specimen is relatively uniform as the latter is a large specimen and local field effects due to finite track dimensions are not considered. We therefore feel that the provision of an enlarged view of the situation close to the specimen will not be of much help for assessing the relative accuracy of the algorithms. The application of algorithm C to finite track dimensions or situations where type I and type II local field effects are present has been reported in references [8] and [9]. An enlarged view of the equipotential distribution and some electron trajectories for a three-electrode structure with local field effects is given in Fig. 16.

AR Dinnis: In all the figures 2 to 6, the odd electron actually penetrates the -2V barrier. Do you not include a means of checking that this happens and take appropriate action?

Authors: Routines have been included in algorithm C to minimise the errors due to electron transition between meshes as mentioned in the last paragraph of section 2.3. Despite this, stray trajectories do occur. As this algorithm is used for quantitative voltage contrast studies in which thousands of electron trajectories are simulated for a particular retarding grid voltage setting (see references [8] and [9]), the occasional couple of odd trajectories do not significantly affect the results. We have found that algorithm C (the linear electric field approach) gives rise to the least stray trajectories compared to the other two algorithms and

this is the algorithm used for our quantitative voltage contrast and indirect specimen charging studies.

DB Holt: In your paper, you claim that your tracking algorithm is more accurate than conventional ones. What is the basis for this claim? Is it purely theoretical or have comparisons of the results obtained with both algorithms been made with experimental results?
Authors: The comparison of the three algorithms were performed through computer simulation studies and a more detailed account of this investigation can be found in reference [11]. We are not aware of any reported experimental verification on the accuracy of electron trajectory algorithms.

K Nakamae: Please explain physical meanings of equations (4) and (6).
Authors: A_x and A_y in equations (4) and (6) are the linear electric field variation coefficients within a particular mesh. We feel that the linear electric field variation within a mesh is a more accurate reflection of the actual situation compared to the constant electric field approach. For situations where the electric field is constant within a mesh, the values of A_x and A_y would be zero.

DB Holt: Your paper describes a nice suite of computer programs. I worry, however, about the problem of reproducibility as I always do in any papers about programs. To be accepted into the body of scientific knowledge, reported facts must be reproducible i.e. any other scientist must be able to repeat the procedures described and get the same result. Clearly it is not possible to rewrite the programs in another laboratory, based on outlines of the underlying principles and be sure that subtle differences will not appear. In the case of Monte Carlo electron trajectory

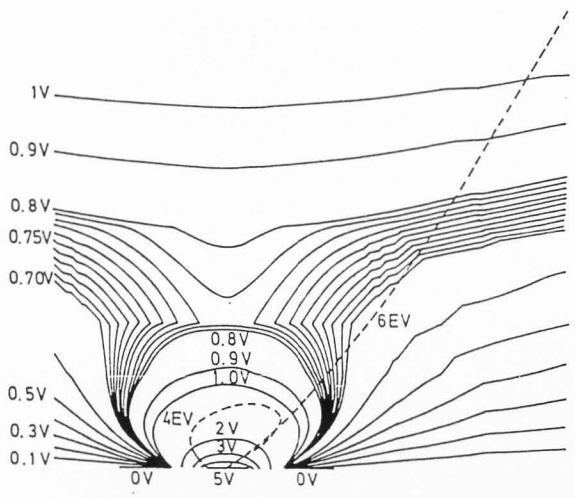

Fig. 16. Potential distribution above a 3-electrode structure in a retarding field energy analyser with voltages (V_1, V_s, V_2) = (0,5,0)V and an extraction field of 10V/mm. Trajectories of a 4eV and 6eV electron are also shown to illustrate the effect of the 4.21V potential barrier.

programs for SEM simulations to run on microcomputers this problem was overcome by 'publishing' the actual software as public domain programs. (This is the case for the well known Joy and Napchan programs - see e.g. D.C. Joy J. Microscopy 143 (1986) pp. 233-248, "The Interpretation of EBIC Images using Monte Carlo Simulations" and E. Napchan and D.B. Holt, in Microscopy of Semiconducting Materials 1987 Conf. Series No. 87 (Inst. Phys., Bristol) pp. 733-738, "Application of Monte Carlo simulations in the SEM Study of Heterojunctions". Both suites of programs have evolved considerably since those papers.) Is there any similar way in which people can gain access to your programs?
Authors: The Monte Carlo and CL models are designed and optimised to run on a IBM 3090 mainframe and NEC SX-1A supercomputer respectively. The programs are still being developed. Interested readers should contact us for details.

DB Holt: As one of the people who pointed out the desirability of basing the modelling of CL signals on Monte Carlo electron trajectory simulations of signal excitation, I am glad that you have written a program to do this. What do you intend to do with the programs? Have you any plans to make experimental measurements yourselves? We would be interested in trying to fit our measurements to curves calculated with your program, e.g. CL intensity vs beam voltage for constant beam power.
Authors: We have performed experiments to measure CL intensity vs beam energies for GaAs specimens. Based on the model, semiconductor parameters have been extracted using the experimental data points. This work has been submitted for publication and is currently under review.

DB Holt: In your CL program you include the effects of both total internal reflection and Fresnel reflection. Can you give an indication of the relative importance of the latter? What fraction of the CL intensity incident on the exit surface that is not totally internal reflected is still lost due to Fresnel reflection?
Authors: Both the total internal reflection and Fresnel loss are a decreasing function of n' where n'=1/n. Fig. 17 shows the calculated discrete average transmissivity T_{av} for different values of n' using equations (30)-(32). The amount of loss through Fresnel reflection, as compared to the total internal reflection, is relatively small, especially for low values of n'. However, it could have a significant impact on samples like GaAs where the refractive index is high. For example in GaAs, about 32.5% of photons incident on the exit surface within the critical angle will still be reflected.

K Nakamae: What differential scattering cross section which characterize the scattering process do you use in the Monte Carlo simulation?
Authors: This Monte Carlo model uses a Rutherford differential scattering cross section.

K Nakamae: How many cubes in the spatial energy dissipation volume do you use in the simulation? How many trajectories do you calculate?

Authors: For a 20 keV beam energy, an array size of (21,21,21) has been used for 0.1 μm of δx, δy and δz to store the energy dissipation. A minimum of 5000 trajectories have been calculated.

K Nakamae: Please explain the physical meaning of equations (21) and (22)?
Authors: In the Berz and Kuiken's formulation [3] for carrier distribution, the method of images was used to implement the boundary condition at the surface which is characterized by a surface recombination velocity. This enables the calculation of the excess minority carrier concentration at any point in the specimen volume. Equations (21) and (22) give the excess carrier density for the cases where $v_s=0$ and ∞ respectively. For $v_s=0$ and ∞, the images are a source and sink respectively.

AR Dinnis: The charging results shown in Fig. 15 are very interesting and significant, despite the approximations needed to make the computations achievable in a realistic time. Do you believe that this technique could be extended to the charging which occurs close to a conductor track lying on the insulating surface of an IC? The availability of such a technique would be very useful in the simulation of accurate trajectories in voltage-contrast spectrometers and could possibly be used to devise a method of laying down charge distribution which would enhance the performance of suitable spectrometers.
Authors: Thank you for the suggestion. Our main objective is to study the effect of specimen charging on voltage measurement in electron beam testers. Preliminary simulation studies have shown that a large proportion of the SEs retarded by the retarding field return to the IC surface. We are now simulating the insulator potential build-up due to these returning SEs.

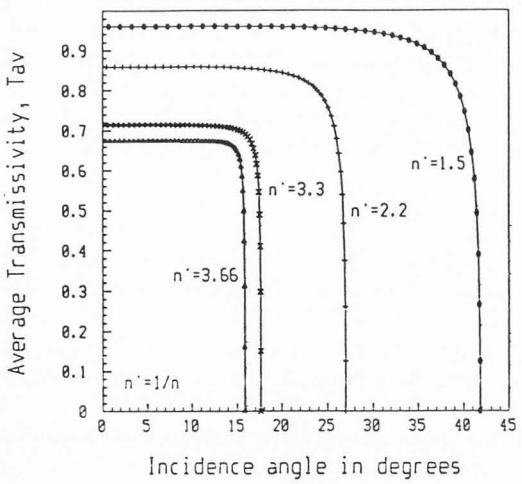

Fig. 17. Transmissivity of randomly polarised photons as a function of the angle of incidence for different values of n calculated using eqns. (30)-(32).

DB Holt: You calculated the effect of "indirect charging" for one case. Have you considered the possibility of calculating the effect of differential charging. This effect is more rapid charging of one part of a specimen than another leading to useful SEM contrast. This was used by B. Wakefield and S. T. Davey (Microscopy of Semiconducting Material 1985 Conf. Series No. 76 (Int. Phys. Bristol) pp. 373-376 "Characterization of Semi-insulating LEC GaAs by SEM"). They found that the centres of the cells of the well-known structure in semi-insulating GaAs charged-up first and this made it possible to see the cell structure in secondary electron images. Could your programs readily cope with such a situation? It would also be interesting to have some idea how widely applicable this technique might be. Does it depend only on resistivity and its percentage variation? Also what is the contrast mechanism? Is it a form of self-induced voltage contrast?
Authors: Thank you for the suggestion. In our indirect charging simulation model, we are concerned primarily with the macro effect of the field generated outside the charged-up specimen. Our simulation model assumes that all insulating materials are homogeneous. At this stage, the model cannot be used to simulate differential charging due to material inhomogeneity.

K Nakamae: Would you comment about the selection of the PE exposure time step of 2.5 seconds in Fig 15 ?
Authors: Fixed charges on the IC package surface modify the field in the cavity region and subsequently influence the SE trajectories. Trial simulations have shown that for PE exposure time less than 2.5 seconds, the amount of fixed charges introduced on the package surface does not significantly deviate the trajectory of a test (2 eV) secondary electron. In Fig. 15, only alternate frames of the potential plots (at intervals of 5 seconds) are shown. The appropriate amendment has been made to the figure caption.

M Schöttler: In your original text, you mentioned that "The PE takes approximately 530 ps to travel a micron distance". We understand this time of 530 ps as the time of flight for a 1 keV electron in free space and so we got another time: 53 fs instead of 530 ps. If this time is not the time of flight in free space we propose to explain how to understand this time.
Authors: The 530 ps is the time of flight of 1 keV beam over a distance of 10 mm (i.e. the distance between the extraction grid and the IC) instead of 1 μm. This error has been amended in the main text. The corrected statement is as follows: "After leaving the plane of the extraction grid, the PE takes approximately 530 ps to reach the specimen (the package is 10 mm below the extraction grid)."